Chapter 12

Analysis of Relaxation Behavior of Free Radicals in Irradiated Cellulose Using Pulse and Continuous-Wave Electron Spin Resonance

Hiromi Kameya and Mitsuko Ukai

Additional information is available at the end of the chapter

http://dx.doi.org/10.5772/75459

1. Introduction

Food is irradiated to destroy harmful bacteria and parasites that might be inadvertently present. Irradiation at lower dose levels also extends shelf-life and can be used to control insects. Irradiation extends the shelf-life of food by retarding maturation in vegetables and reducing spoilage organisms that can grow even under refrigeration. Irradiation can also be used in place of fumigants and other quarantine procedures to import or export fruits and vegetables without the risk of transporting harmful insects.

Electron spin resonance (ESR) studies have reported on induced radicals in irradiated plant foods (Ukai et al., 2006; Ukai & Shimoyama, 2003a, 2003b, 2005; Nakamura et al., 2006; Shimoyama et al., 2006). There are two types of ESR signals from irradiated plant food: one is a singlet with a g-value of nearly 2.0, and the other appears symmetrically as two side signals on both sides of the singlet. The singlet signal has been identified as an organic free radical (Ukai & Shimoyama, 2005).

Clear side signals have been reported in pepper following gamma-ray irradiation (Ukai & Shimoyama, 2003a, 2003b). Similar side signals in wheat flour that contains cellulose and starch are more complicated (Shimoyama et al., 2006; Ukai & Shimoyama, 2005). Side signals have been observed in ginseng that contains a significant amount of fiber (Nakamura et al., 2006) and in irradiated strawberry seeds whose main component is cellulose (Raffi & Stocker, 1996; Raffi & Agnel, 1989). However, only one side signal at the lower magnetic fields has been detected (Raffi & Agnel, 1989). The side signal in the higher magnetic field was considered covered by other stronger ESR signals. These side signals have been named after the "cellulotic radical," because they are observable in ESR spectra of samples containing a significant amount of cellulose (Raffi et al., 2000). Ehrenberg et al. have

reported that the side signals appearing from irradiation were derived from peroxide radicals (Loftroth et al., 1964; A. Ehrenberg et al., 1962). There have been many recent reports on the side signals (Lee et al., 2009; Lee et al., 2008; Yordanov et al., 2009; Raffi et al., 2009; Yamaoki et al., 2009; Sanyal et al., 2008; Cutrubinis et al., 2007; Polovka et al., 2007; Jo & Kwon, 2006; Butz & Hildebrand, 2006).

Lee et al. have reported on irradiated sesame seeds using ESR (Lee et al., 2009; Lee et al., 2008). The report concluded that a pair of ESR lines appears on both sides of the central signal in ESR spectra due to the cellulose radicals formed by ionizing radiation. Yordanov et al. have reported a pair of signals in the irradiated dry medical herbs (Yordanov et al., 2009). A central line and two weak satellite lines were detected. The authors named these after the "cellulose-like" and "carbohydrate-like" triplets (Yordanov et al., 2009). However, their spectra were undefined. Raffi and Yordanov have reported on aromatic herbs, spices, and fruits after irradiation (Raffi et al., 2009). They have also reported a relatively weak triplet.

Polovka et al. have reported on irradiated spices (Polovka et al., 2007). Simulation of ESR spectra for the black pepper samples revealed the formation of three paramagnetic species, i.e., the triplet, doublet assigned to "carbohydrate" radical structures, and the typical three-line "cellulotic" signal. The paramagnetic signals identified in individual irradiated spice samples, along with the spin Hamiltonian parameters, have been employed in quasi-empirical simulations.

A triplet line has been reported from the irradiated flesh of kiwifruits, with the extra signals resulting from cellulose radicals on both sides of the endogenous signal (Jo & Kwon, 2006). Studies on the irradiated shells of walnuts and pistachios have shown that a sample can be unambiguously identified, if beside the central signal satellite peaks, a separation of 6.0 ± 0.05 mT is detected (Butz & Hildebrand, 2006). However, there is little explanation on the origin of the side signals.

With the CW-ESR method, irradiation can be performed using a weak (continuous) microwave field without disturbing the steady state spin system. The pulsed-ESR method employs instantaneous microwave radiation and reorients the spin systems. This can be observed in the absence of a microwave field. Pulsed ESR determines the relaxation behavior of radicals. The relaxation times, T_1 and T_2, were evaluated using the decay of echo signals as a function of time intervals between microwave pulses. However, strict measurement conditions must be met for an accurate analysis of pulsed ESR.

In this study, gamma ray radiation was applied on filter paper that was made of pure cellulose and on an oblate of pure starch which has structure similar to cellulose. We analyzed the ESR side signals originating from these polymers after irradiation. Using theoretical calculations, we simulated the side signals by assuming a triplet signal from the radical at the C(5) position of the glucose unit (Fig. 1 A). This revealed the molecular mechanism of the radical formation. Furthermore, we examined irradiated black pepper using pulsed ESR. Black pepper contains many cellulose and many researchers reported the

radicals in irradiated black pepper using ESR. But there is no report of the measurement of irradiated black pepper containing much cellulose using pulsed ESR. We employed an electron spin echo (ESE) using the pulsed ESR method, i.e., the $\pi/2$- and π-pulse sequence. We measured the relaxation of the spin system and various magnetic parameters such as the g-value and hyperfine couplings.

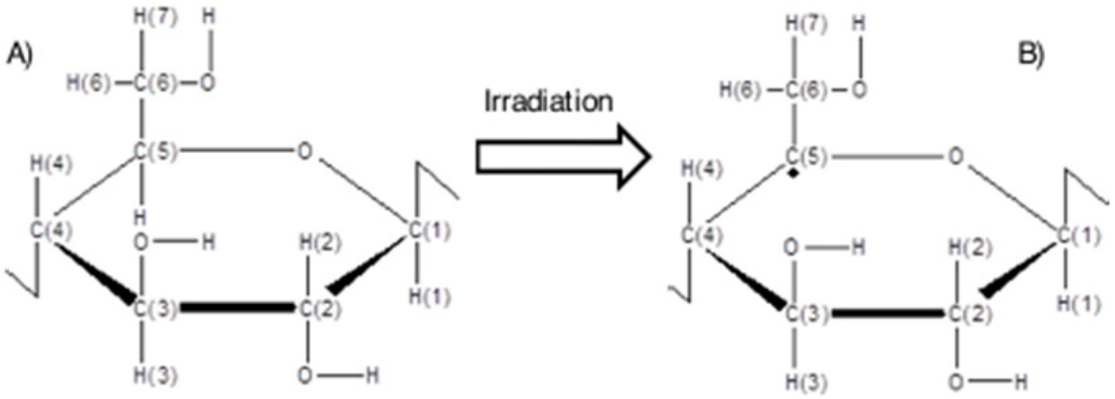

Figure 1. The chemical structure of the cellulose radical. A) before irradiation and B) after irradiation. The triplet ESR spectrum of cellulose is due to the interactions between the two hydrogen atoms at the C6 position of the glucose unit with the unpaired electron formed by the removal of the hydrogen atom at the C5 position of the glucose unit by irradiation

2. Method

2.1. Materials

Filter paper (ADVANTEC MFS., INC) and oblate (Kokko-Oblate Co., Ltd.) were used as samples. The quality of filter paper and oblate used was more than 90% (Japanese Industrial Standards Committee, 1995) cellulose and 99.2% (Kokko-Oblate Co. Ltd.) starch. Black pepper powder which is one of the foods containing much cellulose, commercially available in Japan, was used in the present study. It was bottled in glass and stored at +4.0 °C. After the samples were obtained, they were carefully sealed in a quartz sample tube (99.9% purity; Eiko, Tokyo, Japan). We prepared sample tubes in an argon (Ar) atmosphere and sealed the tubes to remove any oxygen effects (Nakamura et al., 2006). First, the ESR sample tube was degassed for 5 min, and Ar gas was substituted. Then, Ar gas was purged into the ESR sample five times for 2 min each time. The inside pressure of the ESR tube filled with Ar gas was ca. 1 mmHg.

2.2. Irradiation treatment

Irradiation was carried out at the Japan Atomic Energy Research Institute (Takasaki Research Institute) at room temperature (ca. 300 K). We used the gamma-ray originated from ^{60}Co as the irradiation source. The dose rate was 2 kGy/h, and the dose level was controlled by the irradiation time. The irradiation dose levels used were 1, 10, 25, 50, and 100 kGy.

2.3. CW-ESR measurements

CW-ESR measurements were performed with JES-FA100 (JEOL) at 25 °C using the microwave X-band frequency (9.45 GHz). The field modulation frequency was 100 kHz. For the determination of g-values (Swartz et al., 1972), an Mn marker (JEOL) was employed for the correct microwave frequency. In all ESR measurements pertaining to the present study, the magnetic field was swept in the range of 250.0 ± 250.0 mT with a field modulation of 1.0 mT, time constant of 0.03 s, and sweep time of 4 min. When focusing on the single peak at g = 2.00, the magnetic field was swept over the range of 336.5 ± 7.5 mT, with a time constant of 0.03 s and sweep time of 4 min. The side peaks were detected using smaller noise conditions, comprising a field modulation of 1.0 mT. ESR signal parameters were analyzed using the WIN-RAD (Radical Research) software program.

2.4. Pulse-ESR measurements

All pulse-ESR measurements (ESP-380E, Bruker Biospin, Yokohama, Japan) were performed at 25 ◦C. To detect the pulsed electron spin-echo signals, we used a $\pi/2–\pi$ pulse sequence. We used 16 ns for the $\pi/2$ pulse and 24 ns for the π pulse. The pulse interval was 200 ns; recycle delay, 1 ms; and microwave frequency, 9.480 GHz. The electron spin-echo envelope modulation (ESEEM) was measured at the center of the magnetic field (341.5 mT) of the main peak. Theoretically, when the $\pi/2$ pulse is assigned as 16 ns, the corresponding π pulse is 32 ns. We used a shorter pulse, 24 ns, to compensate for the effect of the pin diode on pulse quality. To obtain the echo-detected ESR spectra, the intensity of the electron spin echo was measured as a function of the magnetic field.

2.5. Magnetic interaction tensors

The hyperfine data for two H_α in H_2C_α-C_β fragments were obtained from ENDOR data of irradiated malonic acid (Sagstuen et al., 2000). In the first step, we transformed the tensors into the XYZ axes (Z⊥XY-plane) in terms of the two tensor elements A_{XX} and A_{YY}. These were obtained by standard procedures, assuming an angle (30° slightly idealized).

$$A_{XX} = A_1\cos^2 30^0 + A_2\sin^2 30^0 = -17.95 \text{ G}$$

$$A_{YY} = A_1\sin^2 30^0 + A_2\cos^2 30^0 = -29.05 \text{ G}$$

In the second step, rapid rotation about either X or Y was taken into account.

X: The two H_ζ-tensors both became axially symmetric about X, with $A_\parallel = -17.95$ G. One had Trace (A) = $A_\parallel + 2A_\perp$= (trace invariant under similarity transformation) = $A_1 + A_2 + A_3 = -69.8$ G. Therefore, $A_\perp = -25.9$ G.

Y: The two H_ζ-tensors became axially symmetric about Y, with $A_\parallel = -29.05$ G. By the similar calculation, $A_\perp = -20.4$ G.

Powder spectra for the two models were simulated by an updated version of the KVAPOL program (Thuomas & Lund, 1976).

2.6. Observation of relaxation times of CW-ESR

To determine T_1 and T_2, we used Lund's program (Lund, 2009). For a Gaussian envelope of Lorentzian spin packets, previous treatments have shown the EPR line shape can be expressed as

$$g(r) \propto \frac{B_0\beta}{\Delta B_G}\int_{-\infty}^{\infty}\frac{e^{-(a^2r'^2)dr'}}{t^2+(r-r')^2} \tag{1}$$

which is a convolution of a Gaussian line of width t/a and a Lorentzian line of width t, resulting in a Voigt line profile. Here, β is the transition probability of the line g(r) centered at B_0. The variables r and r′ are defined by the corresponding magnetic fields B and B′ as

$$r = \frac{B-B_0}{\Delta B_L} \qquad r' = \frac{B'-B_0}{\Delta B_L} \tag{2}$$

The parameters a and t^2 affecting the shape of the saturation curve are given by

$$a = \frac{\Delta B_L}{\Delta B_G} \qquad t^2 = 1+\gamma^2 B_1^2 \beta T_1 T_2 = 1+s^2 \tag{3}$$

ΔB_L and ΔB_G are the full widths at half maximum value (FWHM) of the unsaturated Lorentzian and Gaussian line shapes, respectively, and can be expressed in terms of the peak-to-peak widths λ_L and λ_G of the corresponding 1st derivatives as

$$\Delta B_L = (\sqrt{3}/2)\lambda_L \qquad \Delta B_G = \lambda_G/\sqrt{2} \tag{4}$$

The saturation factor s contains the gyromagnetic ratio γ, amplitude of the (left-handed) rotating microwave magnetic field component in the cavity, B_1, and spin-lattice and spin-spin relaxation times T_1 and T_2, respectively. Note that the amplitude B_1 is one-half of the amplitude of the linearly polarized field B_1 in the resonance resonator, as employed experimentally.

The amplitude B1 of the rotating microwave magnetic field component at the sample position of a microwave resonator is related to the input microwave power by an expression of the type

$$B_1 = k\sqrt{Q_L P} = K\sqrt{P} \tag{5}$$

where the constant K depends on the type of resonator and its quality factor Q_L (loaded Q) with the sample in place. It may often be difficult to estimate its value precisely.

Substituting the experimentally measured microwave power P and introducing the spin-relaxation-dependent parameter

$$P_0 = \frac{1}{K^2\gamma^2\beta T_1 T_2} \tag{6}$$

the absorption line shape of equation (1) can be recast to

$$g(r) \propto C\frac{\beta\sqrt{P}}{t}u(ar, at) \tag{7}$$

where the Voigt profile u is the real part of the complex error function w

$$w(z) = exp(-z^2)\, arfc(-iz)\ (w = u + iv, z = at + iar)$$

and

$$t = \sqrt{1 + \beta P / P_0}$$

The procedure to evaluate the line shape function g(r) (equation (7)) numerically, by expanding the function u(ar,at) as the real part of the complex error function, was outlined previously, and was also used in the present work. The code for the Gautschi algorithm, to calculate a Voigt profile as the real part of the complex error function, is a FORTRAN translation of the original ALGOL procedure. To measure the saturation behavior of a single, inhomogenously broadened line, the transition probability β is set to 1 as in a simple two-level system.

Experimentally, the first derivatives of the absorption spectra are recorded, and therefore, the function g(r) has to be differentiated with respect to the variable r (or magnetic field). This was more conveniently done numerically in this work.

The spin-spin relaxation time T_2 is given by definition as $1/\gamma \Delta B_L = 2/\gamma \lambda_L \sqrt{3}$. The estimate of the spin-lattice relaxation time T_1 follows from equation (6) and depends on the factor K to calculate the B_1 field from the corresponding microwave power according to equation (5).

2.7. Observation of relaxation times of pulse-ESR

We used two π/2–τ–π pulse sequences at 16 ns and 24 ns for taking echo measurements. The pulse interval was 200 ns, and the recycle delay was 1.0 ms. For each relaxation measurement, we employed a specific pulse sequence. To determine T_2, we used a two-pulse sequence:

π/2 pulse–τ–π pulse–τ–(echo)

To determine T_1, we used a three-pulse sequence (i.e., the inversion recovery method);

π pulse–τ–π/2 pulse–τ–π pulse–τ–(echo)

We used the same parameter sets as for the spin echo measurements, and fixed τ at 200 ns, to obtain relaxation measurements.

2.8. g-value determination

The g-value was determined independently using the position of the magnetic field and the microwave frequency. For accuracy, the values of the magnetic field and frequency were considered out to the fourth and fifth decimal places, respectively.

3. Results

3.1. Appearance and disappearance of the ESR signals

Figure 2 shows ESR spectra (0 to 500mT) of the filter paper and oblate before and after gamma-ray irradiation. No ESR signals were detected from the two types of samples before irradiation. This suggests the high purity of those samples without an irradiation history.

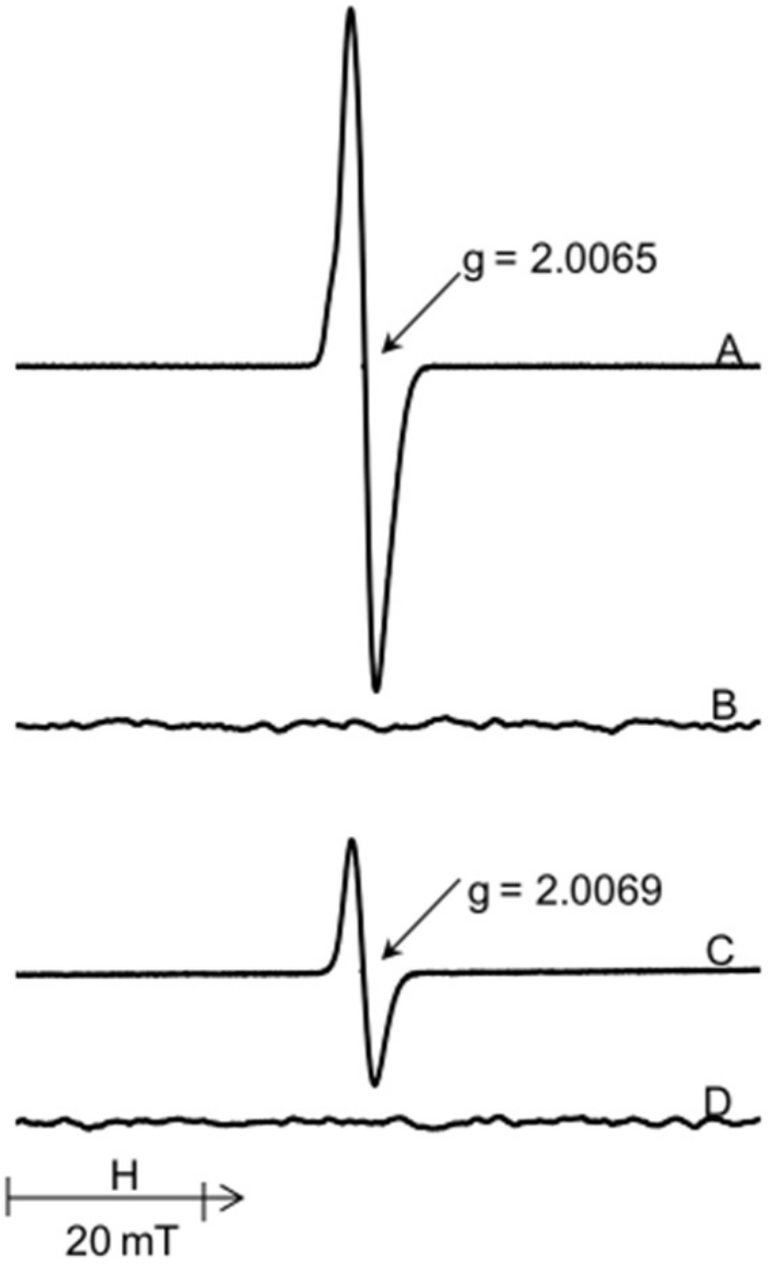

Figure 2. ESR spectra of filter paper and oblate before and after gamma-irradiation. A: irradiated filter paper, B: filter paper, C: irradiated oblate, and D: oblate.

A strong and sharp singlet signal (P_1) was observed near g = 2.0 from the irradiated samples. The g-values of the P_1 signal were identified as g = 2.0065 for the filter paper and g = 2.0069 for the oblate. We have already reported on the ESR singlet signal at g = 2.0 using irradiated ginseng (Nakamura et al., 2006) and black pepper (Ukai & Shimoyama, 2003a, 2003b). These irradiated samples showed two kinds of radicals by ESR analysis: Fe^{3+} at g = 4.0 and Mn^{2+} hyperfine splitting (Swartz et al., 1971). However, irradiated filter paper and irradiated oblate showed neither the Fe^{3+} signal nor Mn^{2+} hyperfine splitting. The signal intensity of P_1 measured from the irradiated filter paper was stronger than that from the irradiated oblate.

Figure 3 shows ESR spectra of the filter paper and oblate followed by irradiation at a magnetic field strength of 329 to 344 mT. In the case of the filter paper, S_1 and S_2 signals were observed at both sides of the P_1 signal. The side signals (S_1 and S_2) were detected at symmetrical positions around the P_1 signal. The g-value of the side signals was found to be 2.0241 for S_1 and 1.9799 for S_2. However, corresponding side signals were not observed in the oblate case.

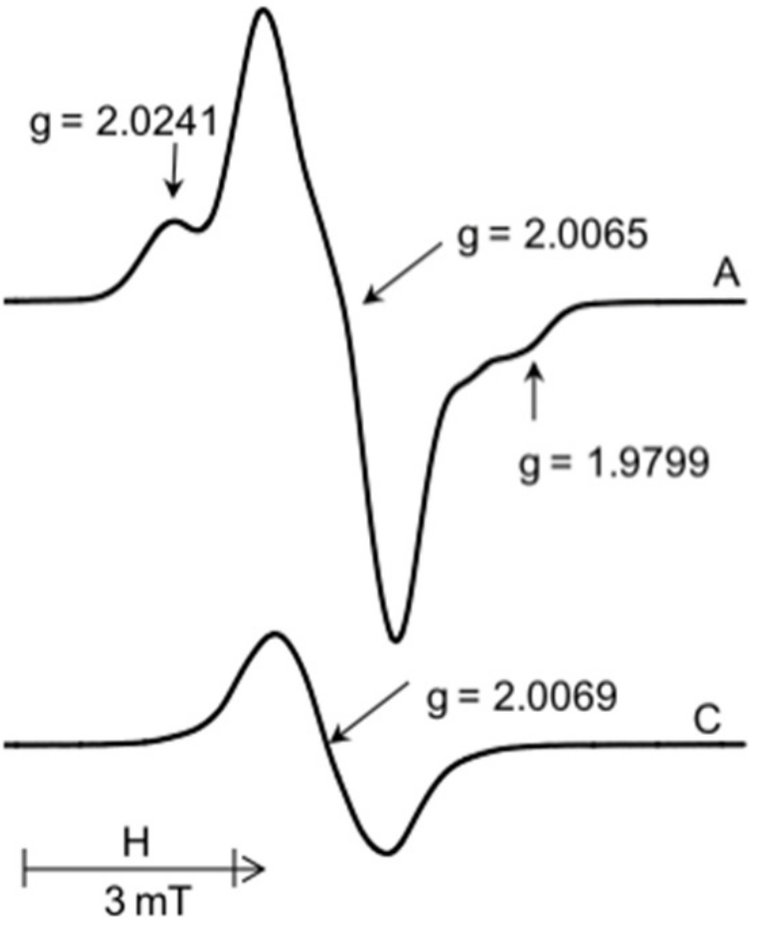

Figure 3. ESR spectra of filter paper and oblate after irradiation. A: irradiated filter paper and C: irradiated oblate.

Experimental evidence (Figs. 2, 3) shows that side signals only appear in cellulose molecules after irradiation. The two side signals occur simultaneously in the ESR spectrum of cellulose. We observed the side signals disappear simultaneously when increasing temperature (Ukai & Shimoyama, 2003b).

Furthermore, according to a monograph on the ESR studies of irradiated polymers (Rånby, 1977), the majority of references have concluded that, among other candidate radicals, a radical at the C(5) position of the glucose unit is the most plausible one in irradiated cellulose. In general, hydrogen abstraction occurs at various chemical bonds by the gamma-irradiation. All the proton sites undergo various chemical reactions simultaneously. However the radical produced at the C(5) position of the glucose unit was comparably stable, so its ESR signal was observable. The stability of the radical was enhanced by the nearby oxygen and alkyl group at the C(6) position of the glucose unit. The ESR signal of the radical at the C(5) position of the glucose unit yields a triplet line shape due to hyperfine interactions between the unpaired electron of a carbon atom and two protons.

Two side signals (S_1 and S_2) were detected in irradiated filter paper (containing cellulose), but not in oblate (containing starch). Therefore, we considered that the side signals were from the cellulose and not from starch. We observed side signals induced by irradiation in botanical foods (Ukai & Shimoyama, 2003a, 2003b, 2005; Shimoyama et al., 2006) and crude drugs (Nakamura et al., 2006) containing cellulose.

Filter paper and oblate consist of cellulose and starch, respectively, and both of them are polysaccharides, represented by the chemical formula $(C_6H_{10}O_5)_n$. Cellulose is a glucose polymer, a β-glucose molecule polymerized by a glycoside bond. Conversely, starch is a polymer produced by polymerizing α-glucose molecules. These structures are different from each other. Cellulose has a sheet-like structure, whereas starch has a helical structure because of the difference in 1, 4 bonds. Thus starch molecules do not form regular sheets and H-bonding is very different. Even though cellulose and starch have similar chemical formulas, their radical formation process may differ due to their structures (Rånby, 1977). It has been reported that the triplet ESR spectrum of cellulose (pure cotton) is due to the equal interaction of the two hydrogen atoms at the C6 position with the unpaired electron formed by the removal of the hydrogen atom at the C5 position of the glucose unit (Rånby, 1977; Arthur, 1971; Arthur & Hinojosa, 1971; Arthur et al., 1966; Baugh et al., 1967) (see Fig. 1 B). The bond breakage at the C5 position may occur only in cellulose. Thus, induction of the side signals should be caused by the strong bonding by β-1, 4 bonds in cellulose.

Upon irradiation, the C5 bond was broken and a radical formed in the cellulose ring (Rånby, 1977). The equivalent two protons located near the unpaired electron at the C5 position of the glucose unit. Thereby, hyperfine interactions occur between the electron spin and the two protons, and the triplet ESR line resulted. The side signals are a part of the triplet. Some interaction between the two protons and the unpaired electron sites at the C2, C3, and C4 positions of the glucose unit are possible, and can be predicted in the cellulose structure (Rånby, 1977; Arthur et al., 1966; Baugh et al., 1967). One needs to consider the physical

three-dimensional structure and energy levels of cellulose bond sites. The irradiated starch samples showed a doublet ESR signal (Rånby, 1977; Adamic, 1968). The unpaired electron in the C5 position of the glucose unit produces the doublet-line spectrum by the hyperfine interaction with H5 (Rånby, 1977; Adamic, 1968).

We revealed the origin of the ESR side signals detected from irradiated filter paper containing pure cellulose. Using theoretical calculations, we further revealed the molecular mechanism of the radical formation of irradiated glucose polymers. The side signals are found to be a precise indicator for irradiation effects in cellulose. They originated from neither the peroxide radical of glucose polymers nor the so-called "cellulotic" radicals. By a simulation method, we proved that the side signals originate from a triplet consisting of a hyperfine interaction with two protons, although the main peak is invisible by an overlapping organic free radical at g = 2.0. Note that we reconfirmed that the simulated spin concentration coincides with the experimental ESR value of 1.7×10^{15} spins/g.

3.2. Molecular motions of radical by simulation

Figure 4 shows experimental ESR as well as the simulated ESR spectra of the radical at the C(5) position of the glucose unit. We simulated the ESR spectra under three different conditions of the radical molecule based upon its molecular structure at the C(5) position of the glucose unit. The first is a spectrum at the rigid limit. In the second case, both C_α-C_β and C_β-H bonds undergo rapid rotations. For the simulation, we employed a set of magnetic parameters such as hfc and g-value tensors as shown Table 1. We used g = 2.0065 and A = 3.0 mT for the radical at the C(5) position of the glucose unit. Because the experimental ESR spectrum indicated a signal with modified hyperfine values, rather than a powder pattern at the rigid limit, we postulated that the radical undergoes rotational motions. In fact, we found through a simulation that the C_α-C_β and C_β-H bonds do undergo simultaneous rotations.

	Rigid limit	C-C rotation	C-C rotation and C-H rotation
g-values	$g_x = 2.0071$	$g^{\perp} = 2.0064$	$g^{\perp} = 2.0064$
	$g_y = 2.0065$	$g^{\perp} = 2.0064$	$g^{\perp} = 2.0064$
	$g_z = 2.0059$	$g_{\circledcirc} = 2.0067$	$g_{\circledcirc} = 2.0067$
Hyperfine splitting (mT)	$A_x = 3.46$	$A^{\perp} = 2.00$	$A^{\perp} = 2.00$
	$A_y = 1.24$	$A^{\perp} = 2.00$	$A^{\perp} = 2.00$
	$A_z = 2.28$	$A_{\circledcirc} = 2.99$	$A_{\circledcirc} = 2.99$
Line shape ratio (L:G)	0:100	0:100	0:100

Table 1. Spectral parameters for simulations

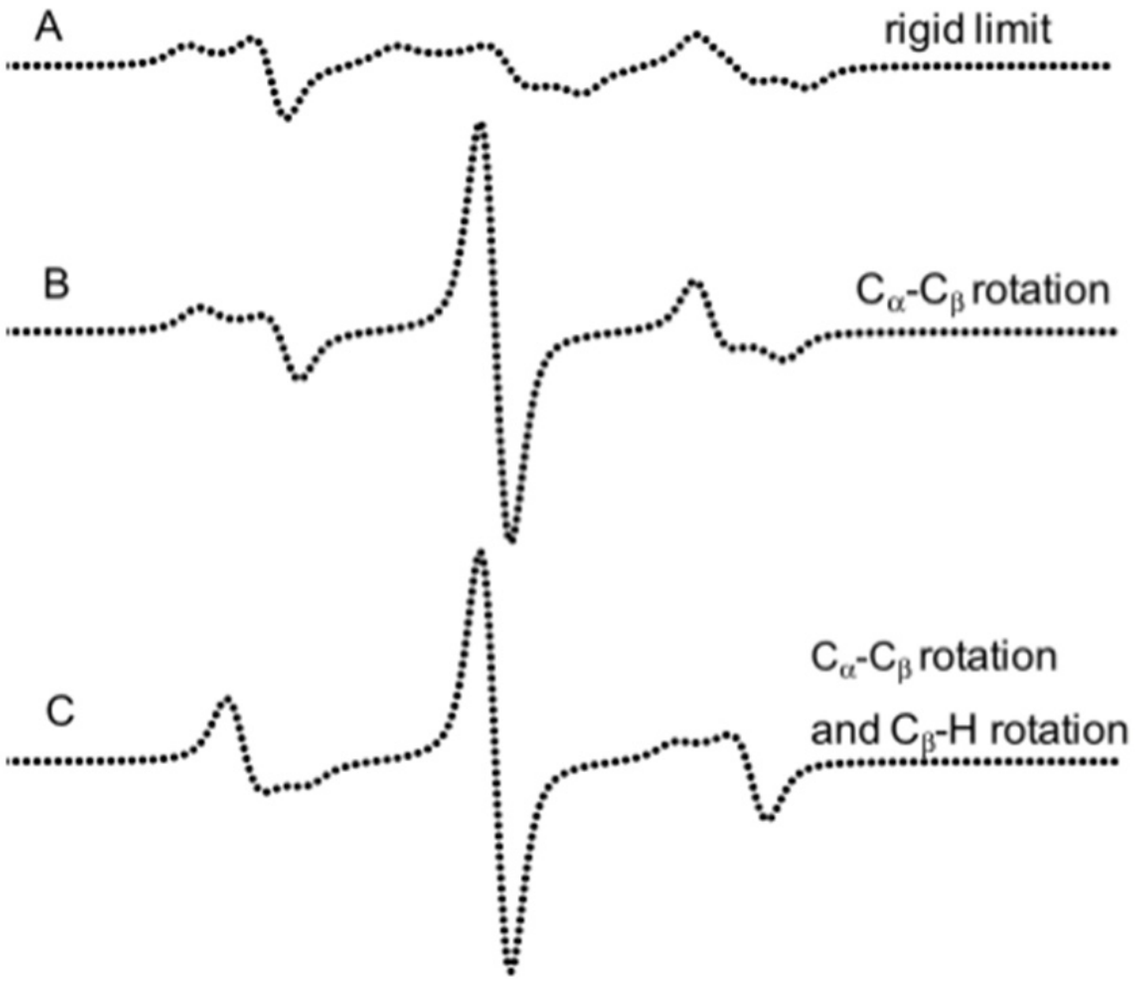

Figure 4. The simulated ESR spectra originated from the radical at the C(5) position of glucose unit under three different conditions of the radical molecule. Experimental ESR spectra of filter paper and oblate after irradiation. A: simulated spectra of rigid limit, B: simulated spectra of C⍟-C⍟ rotation, and C: simulated spectra of C⍟-C⍟ rotation and C⍟-H rotation.

3.3. Field-swept signal of ESE and hyperfine interaction detected by ESEEM

Figure 5 shows a field-swept echo spectrum (shown from 330.0 to 350.0 mT) of the radicals from gamma-ray-irradiated black pepper. We found three peaks: a main peak and two side peaks. An integrator was not used in the present pulse ESR experiment; therefore, the line width of the main peak detected by pulse-ESR was broader than that of the main peak detected by CW-ESR. The signal intensity of the main peak, at g = 2.005, increased with the radiation dosage. Two side peaks were observed when the irradiation doses were higher than 25 kGy. Black pepper contained much cellulose. So, these peaks are due to irradiated cellulose.

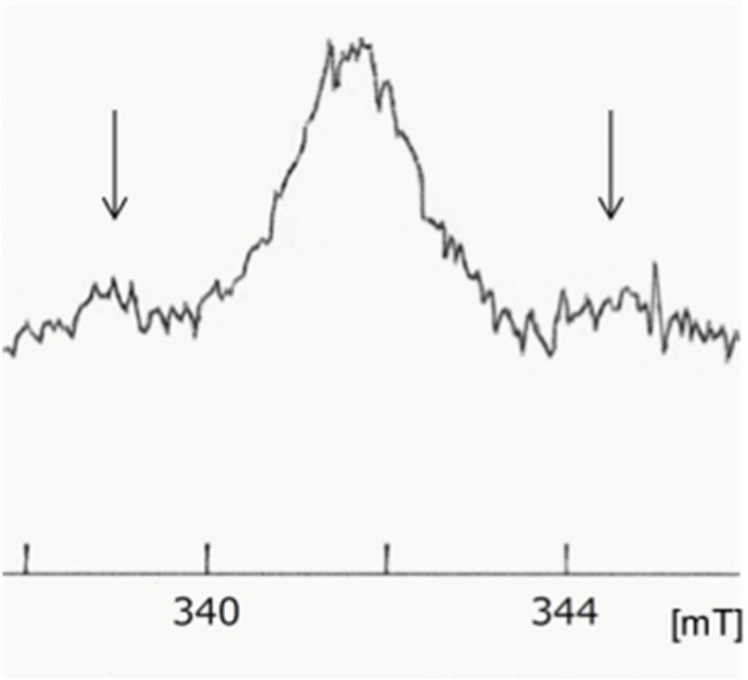

Figure 5. Field-swept (330.0 to 350.0 mT) echo spectrum of gamma-ray-irradiated black pepper at 100 kGy analyzed by pulsed EPR with a microwave frequency of 9.480 GHz. Black pepper powder commercially available in Japan was used. The initial tau value of time between pulses was 200 ns.

The CW-ESR spectra showed 6.0 mT of hyperfine separation between the two side peaks. The field-swept echo yielded a splitting of ca. 6 mT, as shown in Fig. 5. We concluded that both the ESR and the field-swept echo showed the same radical species. We have already reported the corresponding ESR peaks with other specimens using the CW-ESR measurements (Ukai et al., 2006; Ukai & Shimoyama, 2003a, 2003b, 2005; Nakamura et al., 2006; Shimoyama et al., 2006). We observed the same information in the spectra of both pulse- and CW-ESR.

Figure 6 shows a decay signal from the electron spin echo of the gamma-ray-irradiated black pepper sample at the magnetic field position of the main peak (341.5 mT). This echo decay shows ESEEM during the initial time range. ESEEM is also caused by the weak hyperfine interaction between the radiation-induced radicals and remote matrix protons. The two-pulse ESEEM spectra in the present study showed a decay of the observed main peak. The main peak is attributed to oxidized hydroquinone generating paramagnetic semiquinone that exists as an anion or neutral radical. The central peak of the cellulose radical exists in the same position (Kameya et al., 2011).

The peaks in the Fourier-transformed ESEEM spectrum shown in Fig. 6 appeared at 14 MHz and 28 MHz. These peaks are considered to originate from the matrix protons (Astashkin et al., 2000; Gramza et al., 1997). The protons are situated around the radical without being chemically connected. Because this pulse ESR system can detect the interaction between radicals located within a distance of 5 Å, the matrix protons should be situated within 5 Å.

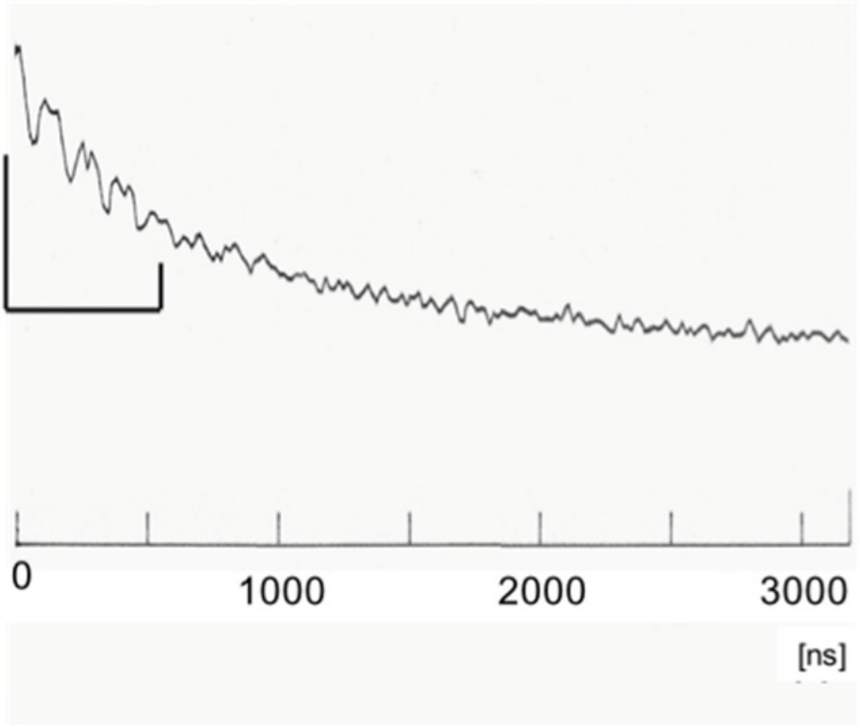

Figure 6. Two-pulse ESEEM time domain spectrum of gamma-ray-irradiated black pepper at 100 kGy with a microwave frequency of 9.480 GHz. Black pepper powder commercially available in Japan was used. The initial tau value of time between pulses was 200 ns.

3.4. Relaxation times, T_1 and T_2

We measured the relaxation times (T_1 and T_2) of the radical at 341.5 mT in the black pepper using the pulsed echo sequence. Table 2 summarizes the relaxation times (T_1 and T_2) of the irradiation-induced radicals in irradiated black pepper. T_1 was calculated using exp(-t/T) as the reverse of the spectrum that corresponds to 1-exp (-t/T). T_1 of the radical produced by 1 kGy of irradiation was 29.7 μs, and T_1 of the radical produced by 100 kGy was 36.0 μs. Relaxation time T_2 was calculated using exp (-t/T), and found to be 276 ns for 1 kGy of irradiation, and 437 ns for 100 kGy of gamma-ray-irradiation. Both the T_1 and T_2 values were enhanced by higher irradiation dosage levels., The relaxation time of the electron spin lattice T_1 depends on several parameters, and this relaxation can occur in various ways, e.g., spin diffusion. We expected the relaxation times to decrease because the dipole interaction (the distance between the radicals) weakened with increasing concentration of irradiation-induced radicals. However, the value of T_1 increased slightly, possibly because of an energy flow through the chemical bonds resulting from radical formation through irradiation. Relaxation time T_2 reflected the interaction among spins. We expected T_2 to decrease with increasing concentration of radicals, i.e., interaction between the radicals by gamma-ray irradiation. However, the values of T_2 were found to increase with the irradiation dose levels. We believe that this interaction between radicals decreased with conformational changes occurring because of bond breakage, caused in turn by the gamma-ray irradiation.

	Pulse-ESR value		CW-ESR value	
Irradiated dose (kGy)	T_1 (×10 ⌠s)	T_2 (×10^2 ns)	T_1 (⌠s)	T_2 (×10^2 ns)
0	3.0	2.8	3.2	1.4
1	3.0	2.9	3.3	1.5
10	3.0	3.5	3.3	1.5
25	3.2	3.5	3.4	1.5
50	3.3	4.2	3.4	1.6

Table 2. Relaxation times (T_1 and T_2) of the radiation induced radicals in irradiated black pepper

In this research, we observed relaxation behaviors of the main singlet peak at 341.5 mT. However, from the theoretical analysis of side peaks, we found that the main singlet peak overlaps with the center peak of the triplet (Kameya et al., 2011). These observations suggest that the carbon-centered radical is responsible for the overlapping of peaks and affects the relaxation times, T_1 and T_2. The relaxation times were also calculated theoretically using the CW-ESR parameter (Lund, 2009). We revealed that T_1 and T_2 from pulsed-ESR and CW-ESR were changed similarly before and after irradiation.

Relaxation times (T_1, T_2) of radicals in black pepper were also measured using pulsed-ESR. T_1 and T_2 were theoretically calculated using the CW-ESR parameter. We used pulsed-ESR and CW-ESR to calculate T_1 and T_2. T_1 and T_2 values increased according to irradiation. We revealed that T_1 and T_2 from pulsed-ESR and CW-ESR were changed similarly before and after irradiation. Before gamma-ray irradiation, no signals were observed in the cellulose. However, after gamma-ray irradiation, a singlet at g = 2.0 was observed, and a pair of side signals appeared simultaneously. Analysis of our theoretical spectra simulation revealed that the hyperfine interactions between the electron spin and the two protons resulted in a triplet ESR line. We compared the experimental spectra with the simulation spectra, and the results corresponded quite closely. We concluded that the twin peaks from the ESR spectra of irradiated cellulose were due to radicals produced at the C(5) site of molecular cellulose.

4. Conclusion

1. We detected ESR side signals from irradiated filter paper containing pure cellulose, and revealed the molecular mechanism of the radical formation of irradiated glucose polymers using theoretical calculations. The side signals are a precise indicator for irradiation effects in cellulose.

2. We postulated that the radical undergoes rotational motions. In simulation, the C_α-C_β and C_β-H bonds undergo simultaneous rotations.
3. We detected the same information in the spectra of both pulse- and CW-ESR. We observed a decay signal from the electron spin echo of the gamma-ray-irradiated black pepper sample at the magnetic field position of the main peak (341.5 mT). This echo decay immediately shows ESEEM during the initial time range.
4. Relaxation times T_1 and T_2 were calculated theoretically using the CW-ESR parameter. We used pulsed-ESR and CW-ESR to calculate T_1 and T_2. We revealed that T_1 and T_2 from pulsed-ESR and CW-ESR were changed similarly before and after irradiation.

Author details

Hiromi Kameya*
National Food Research Institute, Tsukuba-shi, Ibaraki, Japan

Mitsuko Ukai
National Food Research Institute, Tsukuba-shi, Ibaraki, Japan
Hokkaido University of Education, Hakodate-shi, Hokkaid, Japan

5. Acknowledgement

We would like to extend our deepest gratitude to Prof. Anders Lund (Linko¨ping University) and Prof. Sergei A. Dzuba (Institute of Chemical Kinetics and Combustion) for their valuable advice and guidance.

6. References

Adamic, K. (1968). EPR Study of Radicals Generated in Starch by Microwaves or by Conventional Heating. *Starke,* Vol.20, p. 3

Arthur, J. C. Jr. (1971). Cellulose and Cellulose Derarzves. *High Polym.*, Vol.5, pp. 977-990

Arthur, J. C. Jr. & Hinojosa, O. (1971). Oxidative Reactions of Cellulose Initiated by Free Radicals. *J. Polym. Sci.*, Vol.36, pp. 53-71

Arthur J. C.; Mares, J. T.; & Hinojosa, O. (1966). ESR Spectra of Gamma-irradiated Cotton Cellulose I and II. *Text Res. J.*, Vol.36, p. 630

Astashkin, A. V.; Mader, M. L.; Pacheco, A.; Enemark, J. H.; & Raitsimring, A. M. (2000). Characterization of Chloride-depleted Human Sulfite Oxidase by EPR Spectroscopy: Experimental Evidence for the Role of Anions in Product Release. *J. Am. Chem. Soc.*, Vol.122, pp. 5294-5302

* Corresponding Author

Baugh, P. J.; Hinojosa, O.; Arthur, J. C. Jr. (1967). ESR Study of Post-irradiation Reactions of Cellulose and Acrylonitrile. *J. Appl. Polym. Sco.*, Vol.11, p. 1139

Butz, B. & Hildebrand, A. (2006). Bleichen von Walnüssen und Pistazien: Einfluss auf den Bestrahlungsnachweis mittels ESR und GC/MS (Bleaching of Walnuts and Pistachios: Influence on Detection of Irradiation by ESR and GC/MS). *Deutsche Lebensmittel-Rundschau*, Vol.102, No.4, pp. 154-157

Cutrubinis, M.; Chirita, D.; Savu, D.; Secu, C. E.; Mihai, R.; Secu, M.; & Ponta, C. (2007). Preliminary Study on Detection of Irradiated Foodstuffs from the Romanian Market. *Radiat. Phys. Chem.*, Vol.76, No.8-9, pp. 1450-1454

Ehrenberg, A.; Ehrenberg, L.; Loftroth, G. (1962). Radiation-induced Paramagnetic Centers in Plant Seeds at Different Oxygen Concentrations. *Abh. Dtsch. Akad. Der Wiss. Berlin K1. Med.*, Vol.1, pp. 229-231

Gramza, M.; Hilczer, W.; Goslar, J.; & Hoffmann, S. K. (1997). Electron Spin Relaxation and ESEEM Spectroscopy of the Glycine Radical in Diglycine Nitrate Single Crystal. *Acta Chem. Scand.*, Vol.51, pp. 556-561

Japanese Industrial Standards Committee (1995). *Filter Paper for Chemical Analysis*, JIS P3801

Jo, D. & Kwon, H. J. (2006). Detection of Radiation-induced Markers from Parts of Irradiated Kiwifruits. *Food Control.*, Vol.17, No.8, pp. 617-621

Kameya, H.; Nakamura, J.; Ukai, M.; & Shimoyama, Y. (2011). Electron Spin Resonance Spectroscopy of Gamma-Irradiated Glucose Polymers. *Appl. Magn. Reson.*, Vol.40, p. 395

Kokko-Oblate Co., Ltd.: http://www.kokkooblate.co.jp/index.html (2012.3.30)

Lee, J.; Kausar, T.; Chung, H. W.; Jeong, I. Y.; Bhatti, I. A.; & Kwon, J. H. (2009). Properties of PSL, TL and ESR to Identify the Irradiated Sesame Seeds After Steaming. *Food Sci. Biotechnol.*, Vol.18, No.2, pp. 374-378

Lee, J.; Kausar, T.; Kim, B. K.; & Kwon, J. H. (2008). Detection of γ-Irradiated Sesame Seeds Before and After Roasting by Analyzing Photostimulated Luminescence, Thermoluminescence and Electron Spin Resonance. *Jour. Agric. Food Chem.*, Vol.56, No.16, pp. 7184-7188

Loftroth, D.; Ehrenberg, A.; & Ehrenberg, L. (1964). Analysis of Radiation Induced Electron Spin Resonance Spectra in Plant Seeds. *Radiar. Bot.*, Vol.4, pp. 455-467

Lund, A. (2009). Relaxation Time Determination from Continuous-wave Microwave Saturation of EPR Spectra. *Rad. Res.*, Vol.172, pp. 753–760

Nakamura, H.; Ukai, M.; & Shimoyama, Y. (2006). ESR Detection of Wheat Flour Before and After Irradiation. *Spectrochimica Acta*, Vol.63, No.4, pp. 883-887

Polovka, M.; Brezova, V.; & Simko, P. (2007). EPR Spectroscopy: A Tool to Characterise the Gamma Irradiated Foods. *J. Food Nutr. Res.*, Vol.46, No.2, pp. 75-83

Raffi, J. & Agnel, J. P. (1989). Electron Spin Resonance Identification of Irradiated Fruits. *Radiat. Phys. Chem.*, Vol.34, pp. 891-894

Raffi, J. & Stocker, P. (1996). Electron Paramagnetic Resonance Detection of Irradiated Foodstuffs. *Appl. Magn. Reson.*, Vol.10, pp. 357-373

Raffi, J.; Yordanov, N. D.; Chabane, S.; Douifi, L.; & Gancheva, V. (2000). Identification of Irradiation Treatment of Aromatic Herbs, Spices and Fruits by Electron Paramagnetic Resonance and Thermoluminescence. *Spectrochimica Acta*, Vol.63, No.4, pp. 409-416

Raffi, J.; Yordanov, N. D.; Chabane, S.; Douifi, L.; Gancheva, V.; & Ivanova, S. (2009). Identification of Irradiation Treatment of Aromatic Herbs, Spices and Fruits by Electron Paramagnetic Resonance and Thermoluminescence. *Spectrochimica Acta*, Vol.56, pp. 409-416

Rånby, B. (1977). *ESR Spectroscopy in Polymer Research*, Springer-Verlag, Berlin and Heidelberg, pp. 235-240

Sagstuen, E.; Lund, A.; & Maruani, J. (2000). Weakly Coupled Proton Interactions in the Malonic Acid Radical: Single Crystal ENDOR Analysis and EPR Simulation at Microwave Saturation. *J. Phys. Chem.*, Vol.104, pp. 6362-6371

Sanyal, B.; Sajilata, M. G.; Chatterjee, S.; Singhal, R. S.; Variyar, P. S.; Kamat, M. Y.; & Sharma, A. (2008). Identification of Irradiated Cashew Nut by Electron Paramagnetic Resonance Spectroscopy. *J. Agric. Food Chem.*, Vol.56, No.19, pp. 8987-8991

Shimoyama, Y.; Nakamura, H.; & Ukai, M. (2006). Free Radical Irradiated Wheat Flour Detected by Electron Spin Resonance Spectroscopy. *Spectrochimica Acta*, Vol.63, No.4, pp. 888-890

Swartz, M. H.; Bolton, J. R.; & Borg, C. D. (1972). *Biological Applications of Electron Spin Resonance*, John Wiley & Sons, Inc., New York, pp. 23-29

Thuomas, K. Å. & Lund, A. (1976). Analysis of EPR with Large Quadrupole Interaction. *J. Magn. Reson.*, Vol.22, pp. 315-325

Ukai, M.; Nakamura, H.; & Shimoyama, Y. (2006). An ESR Protocol based on Relaxation Phenomena in Irradiated Foods. *Spectrochimica Acta*, Vol.A63, pp. 879-882

Ukai, M. & Shimoyama, Y. (2003). An Electron Spin Resonance Study of Evolution of Organic Free Radicals in Irradiated Pepper. *J. Food Sci.*, Vol.68, No.7, pp. 2225-2229

Ukai, M. & Shimoyama, Y. (2003). Free Radicals in Irradiated Pepper: An Electron Spin Resonance Study. *Appl. Magn. Reson.*, Vol.24, pp. 1-11

Ukai, M. & Shimoyama, Y. (2005). Free Radicals in Irradiated Wheat Flour Detected by Electron Spin Resonance. *Appl. Magn. Reson.*, Vol.29, pp. 315-324

Yamaoki, R.; Tsujino, T.; Kimura, S.; Mino, Y.; & Ohta, M. (2009). Detection of Organic Free Radicals in Irradiated Foeniculi fructus by Electron Spin Resonance Spectroscopy. *J. Nat. Med.*, Vol.63, No.1, pp. 28-31

Yordanov, N. D.; Lagunov, O.; & Dimov, K. (2009). EPR Spectra Induced by Gamma-irradiation of Some Dry Medical Herbs. *Radiat. Phys. Chem.*, Vol.78, No.4, pp. 277-280

IntechOpen